15. Skotheim, T. A. *Handbook of Conducting Polymers* (Dekker, New York, 1986).
16. Bard, A. J. & Faulkner, L. A. *Electrochemical Methods—Fundamentals and Applications* (Wiley, New York, 1984).
17. Xing, K. Z., Fahlman, M., Chen, X. W., Inganäs, O. & Salaneck, W. R. The electronic structure of poly(3,4-ethylene-dioxyghiophene): studied by XPS and UPS. *Synth. Met.* **89,** 161–165 (1997).
18. Brown, T. M. *et al.* Built-in field electroabsorption spectroscopy of polymer light-emitting diodes incorporating a doped poly(3,4-ethylene dioxythiophene) hole injection layer. *Appl. Phys. Lett.* **75,** 1679–1681 (1999).
19. Dietrich, M. & Heinze, J. Poly(4,4′-Dimethoxybithiophene)—A new conducting polymer with extraordinary redox and optical properties. *Synth. Met.* **41–43,** 503–506 (1991).
20. Malliaras, G. G. & Scott, J. C. Numerical simulations of the electrical characteristics and the efficiencies of single-layer organic light emitting diodes. *J. Appl. Phys.* **85,** 7426–7432 (1999).
21. Malliaras, G. G., Salem, J. R., Brock, P. J. & Scott, C. Electrical characteristics and efficiency of single-layer organic light-emitting diodes. *Phys. Rev. B* **58,** R13411–R13414 (1998).

Acknowledgements

We thank J. Heinze for making some bithiophene available, W. Brütting for discussions, and Bayer AG (Leverkusen, Germany) for the donation of Baytron P.

Correspondence and requests for materials should be addressed to K.M. (e-mail: klaus.meerholz@cup.uni-muenchen.de).

Selection of peptides with semiconductor binding specificity for directed nanocrystal assembly

Sandra R. Whaley*, D. S. English*, Evelyn L. Hu†, Paul F. Barbara*‡ & Angela M. Belcher*‡

** Department of Chemistry and Biochemistry, ‡ The Texas Materials Institute, The University of Texas at Austin, Austin, Texas 78712, USA*
†Center for Quantized Electronic Structures, University of California, Santa Barbara, California 93106, USA

In biological systems, organic molecules exert a remarkable level of control over the nucleation and mineral phase of inorganic materials such as calcium carbonate and silica, and over the assembly of crystallites and other nanoscale building blocks into complex structures required for biological function[1–4]. This ability to direct the assembly of nanoscale components into controlled and sophisticated structures has motivated intense efforts to develop assembly methods that mimic or exploit the recognition capabilities and interactions found in biological systems[5–10]. Of particular value would be methods that could be applied to materials with interesting electronic or optical properties, but natural evolution has not selected for interactions between biomolecules and such materials. However, peptides with limited selectivity for binding to metal surfaces and metal oxide surfaces have been successfully selected[10,11]. Here we extend this approach and show that combinatorial phage-display libraries can be used to evolve peptides that bind to a range of semiconductor surfaces with high specificity, depending on the crystallographic orientation and composition of the structurally similar materials we have used. As electronic devices contain structurally related materials in close proximity, such peptides may find use for the controlled placement and assembly of a variety of practically important materials, thus broadening the scope for 'bottom-up' fabrication approaches.

Phage-display libraries, based on a combinatorial library of random peptides—each containing 12 amino acids—fused to the pIII coat protein of M13 coliphage[12], provided us with $\sim 10^9$ different peptides that were reacted with crystalline semiconductor structures. Five copies of the pIII coat protein are located on one end of the phage particle, accounting for 10–16 nm of the particle. The phage-display approach provided a physical linkage between the peptide–substrate interaction and the DNA that encodes that interaction. The experiments described here utilized five different single-crystal semiconductors: GaAs(100), GaAs(111)A, GaAs(111)B, InP(100) and Si(100). These substrates allowed for systematic evaluation of the peptide–substrate interactions. Protein sequences that successfully bound to the specific crystal were eluted from the surface, amplified by 10^6, and re-reacted against the substrate under more stringent conditions. This procedure was repeated five times to select the phage with the most specific binding. After the third, fourth and fifth rounds of phage selection, crystal-specific phage were isolated and their DNA sequenced. We identified peptide binding that is selective for the crystal composition (for example, binding to GaAs but not to Si) and crystalline face (for example, binding to (100) GaAs, but not to (111)B GaAs).

Twenty clones selected from GaAs(100) were analysed to determine epitope binding domains to the GaAs surface. The partial peptide sequences of the modified pIII protein are shown in Fig. 1, revealing similar amino-acid sequences among peptides exposed to GaAs. With increasing number of exposures to a GaAs surface, the number of uncharged polar and Lewis-base functional groups increased. Phage clones from third, fourth and fifth round sequencing contained on average 30%, 40% and 44% polar functional groups, respectively, while the fraction of Lewis-base functional groups increased at the same time from 41% to 48% to 55%. The observed increase in Lewis bases, which should constitute only 34% of the functional groups in random 12-mer peptides from our library, suggests that interactions between Lewis bases on the peptides and Lewis-acid sites on the GaAs surface may mediate the selective binding exhibited by these clones.

The expected structure of the modified 12-mers selected from the library would be an extended conformation, which seems likely for

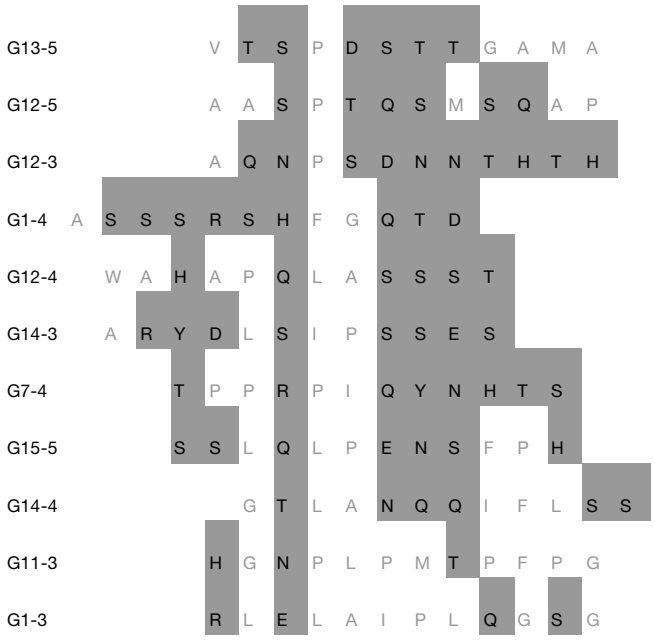

Figure 1 Selected amino-acid sequences of randomized peptide inserts. Here we show partial amino-acid sequences from clones that bound to GaAs(100). These sequences have amino acids with functional groups that can donate electrons to the GaAs surface (shaded areas). Serine (S) and threonine (T) both have hydroxyl side chains that differ by one carbon. Asparagine (N) and glutamine (Q) both have amine-bearing side chains that differ by one carbon. Non-polar amino acids are indicated by grey lettering. The clones were named as follows: G1-3 was the first clone selected from GaAs (100) during the third round of selection.

small peptides, making the peptide much longer than the unit cell (5.65 Å) of GaAs. Therefore, only small binding domains would be necessary for the peptide to recognize a GaAs crystal. These short peptide domains, highlighted in Fig. 1, contain serine- and threonine-rich regions in addition to the presence of amine Lewis bases, such as asparagine and glutamine. To help elucidate the exact binding sequence, we have begun screening our surfaces with shorter libraries, including 7-mer and disulphide constrained 7-mer libraries. By reducing the size and flexibility of the binding domain, fewer peptide–surface interactions are allowed, thereby increasing the strength of interactions between generations of selection.

Phage, tagged with streptavidin-labelled 20-nm colloidal gold particles bound to the phage through a biotinylated antibody to the M13 coat protein, were used for quantitative assessment of specific binding. X-ray photoelectron spectroscopy (XPS) elemental composition determination was performed, monitoring the phage–substrate interaction through the intensity of the gold 4*f*-electron signal (Fig. 2a–c). Without the presence of the G1-3 phage, the antibody and the gold streptavidin did not bind to the GaAs(100) substrate. The gold binding was, therefore, specific to the phage and an indicator of the phage binding to the substrate.

Using XPS we showed that the G1-3 clone isolated from GaAs(100) bound specifically to GaAs(100) but not to Si(100) (see Fig. 2a). In complementary fashion the S1 clone, screened against the (100) Si surface, showed poor binding to the (100) GaAs surface. Some GaAs clones also bound the surface of InP (100), another zinc-blende structure. The basis of the selective binding, whether it is chemical, structural or electronic, is still under investigation. In addition, the presence of native oxide on the substrate surface could alter the selectivity of peptide binding.

The preferential binding of the G1-3 clone to GaAs(100), over the (111)A (gallium terminated) or (111)B (arsenic terminated) face of GaAs was shown (Fig. 2b, c). The G1-3 clone surface concentration was greater on the (100) surface, which was used for its selection, than on the gallium-rich (111)A or arsenic-rich (111)B surfaces. These different surfaces are known to exhibit different chemical reactivities, and it is not surprising that there is selectivity demonstrated in the phage binding to the various crystal faces. Although the bulk termination of both 111 surfaces give the same geometric structure, the differences between having Ga or As atoms outermost in the surface bilayer become more apparent when comparing surface reconstructions. The composition of the oxides of the various GaAs surfaces is also expected to be different, and this in turn may affect the nature of the peptide binding.

In Fig. 2c, we plot the intensity of Ga 2*p* electrons against the binding energy from substrates that were exposed to the G1-3 phage clone. As expected from the results in Fig. 2b, the Ga 2*p* intensities observed on the GaAs (100), (111)A and (111)B surfaces are inversely proportional to the gold concentrations. This decrease in Ga 2*p* intensity on surfaces with higher gold concentrations was due to the increase in surface coverage by the phage. XPS is a surface technique with a sampling depth of approximately 30 Å; therefore,

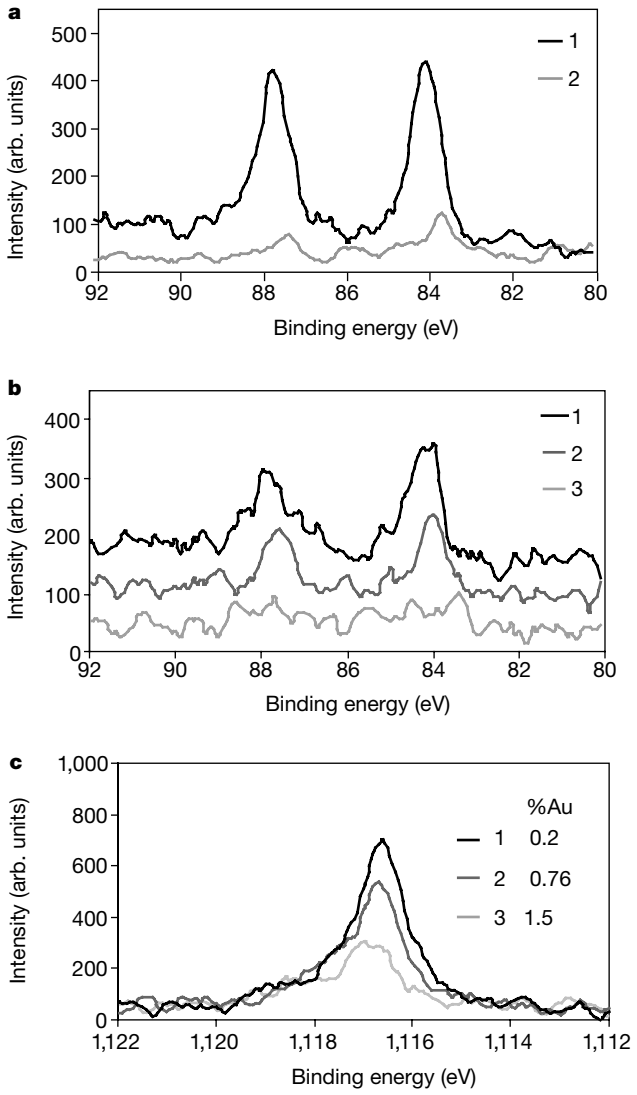

Figure 2 Detection of gold-labelled phage on GaAs using X-ray photoelectron spectroscopy. **a**, Plot of Au 4*f* binding energy versus intensity for the G1-3 clone on GaAs(100) (curve 1) and Si(100) (curve 2) surfaces. **b**, As **a** but for the following surfaces: GaAs(100) (curve 1), GaAs(111)A (curve 2), and GaAs(111)B (curve 3). **c**, Plot of Ga 2*p* binding energy versus intensity for the G1-3 clone on the following surfaces: GaAs(111)B (curve 1), GaAs(111)A (curve 2), and GaAs(100) (curve 3).

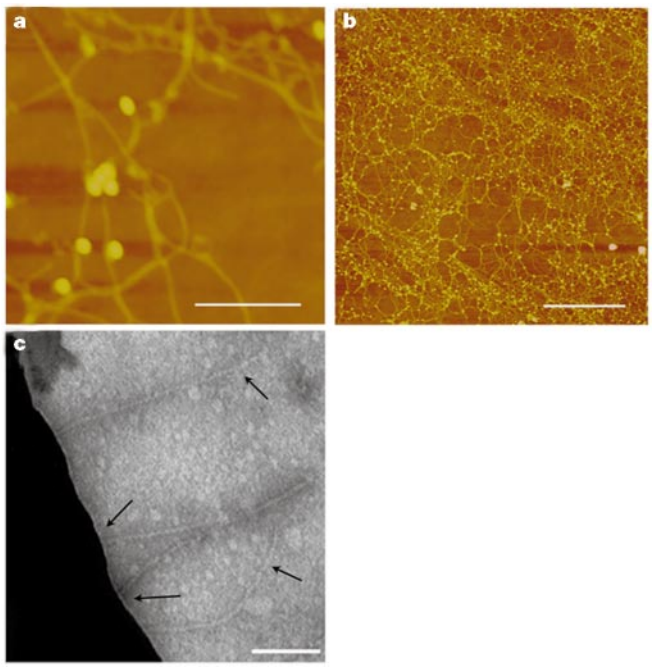

Figure 3 AFM and TEM analysis of peptide–semiconductor recognition. **a**,**b**, AFM images of G1-3 phage bound to an InP(100) substrate. **a**, Individual phage and their attached Au nanoparticles. Scale bar, 250 nm. **b**, Image showing the uniformity of phage coverage on the InP surface. Scale bar, 2.5 μm. **c**, TEM image of G1-3 phage recognition of GaAs. Individual phage particles are indicated with arrows. Scale bar, 500 nm.

as the thickness of the organic layer increases, the signal from the inorganic substrate decreases. This observation was used to confirm that the intensity of gold was indeed due to the presence of phage on the surface of GaAs.

Binding studies were performed that correlate with the XPS data, where equal numbers of specific phage clones were exposed to various semiconductor substrates with equal surface areas. Wild-type clones (no random peptide insert) did not bind to GaAs (no plaques were detected). For the G1-3 clone, the eluted phage population was 12 times greater from GaAs(100) than from the GaAs(111)A surface.

Using atomic force microscopy (AFM), we imaged the G1-3, G12-3 and G7-4 clones bound to GaAs(100) and InP(100). The InP crystal has a zinc-blende structure, isostructural with GaAs, although the In–P bond has greater ionic character than the Ga–As bond[13]. The 10-nm width and 900-nm length of the observed phage in AFM matches the dimensions of the M13 phage observed by transmission electron microscopy (TEM), and the gold spheres bound to M13 antibodies were observed bound to the phage (Fig. 3a). As shown in Fig. 3b, the InP surface has a high concentration of phage. These images suggest that there are many factors involved in substrate recognition, including atom size, charge, polarity and crystal structure.

The G1-3 clone (negatively stained) is shown bound to a GaAs crystalline wafer (dark in colour) in the TEM image in Fig. 3c. The arrows indicate individual phage particles, bound through the pIII minor coat protein located at one end of the phage clone. This image confirms that binding was directed by the modified pIII protein of G1-3, not through non-specific interactions with the major coat protein. This illustrates the feasibility of using specific peptide–semiconductor interactions in assembling nanostructures and heterostructures (Fig. 4e).

We used fluorescence microscopy to demonstrate the preferential attachment of phage to a zinc-blende surface in close proximity to a surface of differing chemical and structural composition. A nested square pattern was etched into a GaAs wafer; this pattern contained 1-μm lines of GaAs, and 4-μm SiO_2 spacings in between each line, (Fig. 4a, b). The G12-3 clones were interacted with the GaAs/SiO_2 patterned substrate, washed to reduce non-specific binding, and tagged with an immuno-fluorescent probe, tetramethyl rhodamine (TMR). The tagged phage are seen as the three red lines and the centre dot, in Fig. 4b, corresponding to G12-3 binding only to GaAs. The SiO_2 regions of the pattern remain unbound by phage and are dark in colour. This result was not observed on a control that was not exposed to phage, but which was exposed to the primary antibody and TMR (Fig. 4a).

We observed that the GaAs clone G12-3 was substrate-specific for GaAs over AlGaAs (Fig. 4c). AlAs and GaAs have essentially identical lattice constants at room temperature, 5.66 Å and 5.65 Å, respectively, and thus ternary alloys of $Al_xGa_{1-x}As$ can be epitaxially grown on GaAs substrates. GaAs and AlGaAs have zinc-blende crystal structures, but the G12-3 clone exhibited selectivity in binding only to GaAs. A multilayer substrate was used, consisting of alternating layers of GaAs and of $Al_{0.98}Ga_{0.02}As$. The substrate material was cleaved and subsequently reacted with the G12-3 clone. The G12-3 clones were labelled with 20-nm gold nanoparticles. Examination by scanning electron microscopy (SEM) shows the alternating layers of GaAs and $Al_{0.98}Ga_{0.02}As$ within the heterostructure (Fig. 4c). X-ray elemental analysis of gallium and aluminium was used to map the gold particles exclusively to the GaAs layers of the heterostructure, demonstrating the high degree of binding specificity for chemical composition. In Fig. 4d, we provide a model for the discrimination of phage for semiconductor heterostructures, as seen in the fluorescence and SEM images (Figs 4a–c).

We have shown the power of using phage-display libraries to identify, develop and amplify binding between organic peptide sequences and inorganic semiconductor substrates. Experimental work remains to be performed, including computer simulations to understand better the nature of the peptide–substrate binding demonstrated by these experiments. We have extended this peptide recognition and specificity of inorganic crystals to other substrates, including GaN, ZnS, CdS, Fe_3O_4 and $CaCO_3$; these results will be reported elsewhere. We are currently designing bivalent synthetic peptides with two-component recognition (Fig. 4e); such peptides have the potential to direct nanoparticles to specific locations on a semiconductor structure. These organic–inorganic pairs should provide powerful building blocks for the fabrication of a new generation of complex, sophisticated electronic structures. □

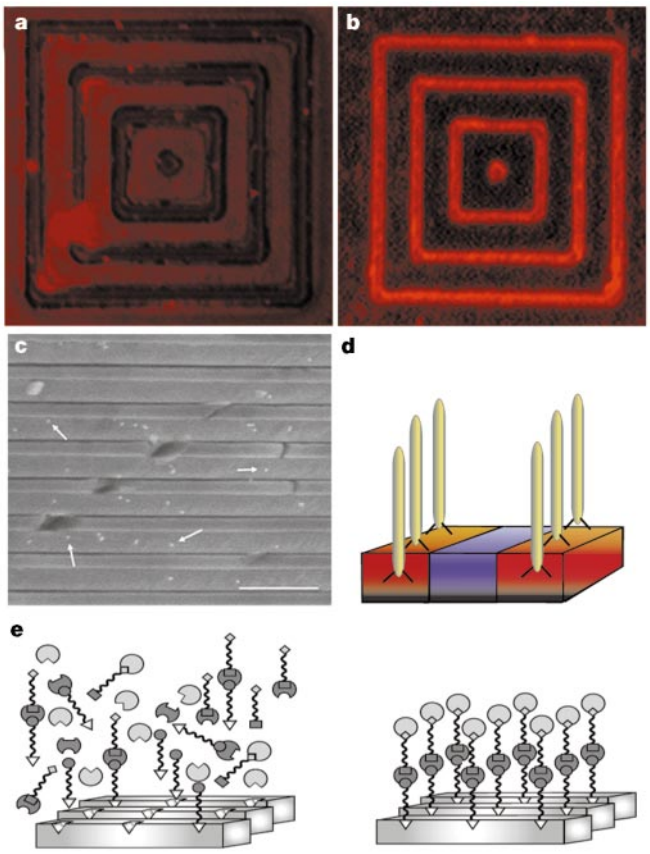

Figure 4 Phage recognition of semiconductor heterostructures. **a**–**c**, Fluorescence images related to GaAs recognition by phage. **a**, Control experiment: no phage is present, but primary antibody and streptavidin-tetramethyl rhodamine (TMR) are present. **b**, The GaAs clone G12-3 was interacted with a substrate patterned with 1-μm GaAs lines and 4-μm SiO_2 spaces. The phage were then fluorescently labelled with TMR. The G12-3 clone specifically recognized the GaAs and not the SiO_2 surface; scale bar, 4 μm. A diagram of this recognition process is shown in **d**, in which phage specifically attach to one semiconductor rather than another, in a heterostructure. **c**, An SEM image of a heterostructure containing alternating layers of GaAs and $Al_{0.98}Ga_{0.02}As$, used to demonstrate that this recognition is element-specific. The cleaved surface was interacted with G12-3 phage, and the phage was then tagged with 20-nm gold particles. These nanoparticles (shown arrowed in **c**) are located on GaAs and not AlGaAs layers. Scale bar, 500 nm. **e**, Diagram illustrating the use of this specificity to design nanoparticle heterostructures using proteins with multiple recognition sites.

Methods

Peptide selection

The library was exposed to the semiconductor crystals in Tris-buffered saline (TBS) containing 0.1% TWEEN-20, to reduce phage–phage interactions on the surface. After rocking for 1 h at room temperature, the surfaces were washed with 10 exposures to Tris-buffered saline, pH 7.5, and increasing TWEEN-20 concentrations from 0.1% to 0.5% (v/v). The phage were eluted from the surface by the addition of glycine–HCl (pH 2.2) for

10 min, transferred to a fresh tube and then neutralized with Tris–HCl (pH 9.1). The eluted phage were titred and binding efficiency was compared.

The phage eluted after third-round substrate exposure were mixed with their *Escherichia coli* ER2537 host and plated on LB XGal/IPTG plates. Since the library phage were derived from the vector M13mp19, which carries the lacZα gene, phage plaques were blue in colour when plated on media containing Xgal (5-bromo-4-chloro-3-indoyl-β-D-galactoside) and IPTG (isopropyl-β-D-thiogalactoside). Blue/white screening was used to select phage plaques with the random peptide insert. Plaques were picked and DNA sequenced from these plates.

Substrate preparation

Substrate orientations were confirmed by X-ray diffraction, and native oxides were removed by appropriate chemical specific etching. The following etches were tested on GaAs and InP surfaces: NH_4OH: H_2O 1:10, HCl:H_2O 1:10, H_3PO_4: H_2O_2: H_2O 3:1:50 at 1 min and 10 min etch times. The best element ratio and least oxide formation (using XPS) for GaAs and InP etched surfaces was achieved using HCl: H_2O for 1 min followed by a deionized water rinse for 1 min. However, since an ammonium hydroxide etch was used for GaAs in the initial screening of the library, this etch was used for all other GaAs substrate experiments. Si(100) wafers were etched in a solution of HF:H_2O 1:40 for one minute, followed by a deionized water rinse. All surfaces were taken directly from the rinse solution and immediately introduced to the phage library. Surfaces of control substrates, not exposed to phage, were characterized and mapped for effectiveness of the etching process and morphology of surfaces by AFM and XPS.

Multilayer substrates of GaAs and of $Al_{0.98}Ga_{0.02}As$ were grown by molecular beam epitaxy onto (100) GaAs. The epitaxially grown layers were Si-doped (n-type) at a level of 5×10^{17} cm^{-3}.

Antibody and gold labelling

For the XPS, SEM and AFM experiments, substrates were exposed to phage for 1 h in Tris-buffered saline then introduced to an anti-fd bacteriophage—biotin conjugate, an antibody to the pIII protein of fd phage, (1:500 in phosphate buffer, Sigma) for 30 min and then rinsed in phosphate buffer. A streptavidin/20-nm colloidal gold label (1:200 in phosphate buffered saline (PBS), Sigma) was attached to the biotin conjugated phage through a biotin–streptavidin interaction; the surfaces were exposed to the label for 30 min and then rinsed several times with PBS.

XPS

The following controls were done for the XPS experiments to ensure that the gold signal seen in XPS was from gold bound to the phage and not non-specific antibody interaction with the GaAs surface. The prepared (100) GaAs surface was exposed to (1) antibody and the streptavidin–gold label, but without phage, (2) G1-3 phage and streptavidin–gold label, but without the antibody, and (3) streptavidin–gold label, without either G1-3 phage or antibody.

The XPS instrument used was a Physical Electronics Phi ESCA 5700 with an aluminium anode producing monochromatic 1,487-eV X-rays. All samples were introduced to the chamber immediately after gold-tagging the phage (as described above) to limit oxidation of the GaAs surfaces, and then pumped overnight at high vacuum to reduce sample outgassing in the XPS chamber.

AFM

The AFM used was a Digital Instruments Bioscope mounted on a Zeiss Axiovert 100s-2tv, operating in tip scanning mode with a G scanner. The images were taken in air using tapping mode. The AFM probes were etched silicon with 125-μm cantilevers and spring constants of 20–100 $N\,m^{-1}$ driven near their resonant frequency of 200–400 kHz. Scan rates were of the order of 1–5 $\mu m\,s^{-1}$. Images were levelled using a first-order plane fit to remove sample tilt.

TEM

TEM images were taken using a Philips EM208 at 60 kV. The G1-3 phage (diluted 1:100 in TBS) were incubated with GaAs pieces (500 μm) for 30 min, centrifuged to separate particles from unbound phage, rinsed with TBS, and resuspended in TBS. Samples were stained with 2% uranyl acetate.

SEM

The G12-3 phage (diluted 1:100 in TBS) were incubated with a freshly cleaved heterostructure surface for 30 min and rinsed with TBS. The G12-3 phage were tagged with 20-nm colloidal gold. SEM and elemental mapping images were collected using the Norian detection system mounted on a Hitachi 4700 field emission scanning electron microscope at 5 kV.

Received 16 November 1999; accepted 10 April 2000.

1. Belcher, A. M. *et al.* Control of crystal phase switching and orientation by soluble mollusc-shell proteins. *Nature* **381,** 56–58 (1996).
2. Falini, G. *et al.* Control of aragonite or calcite polymorphism by mollusk shell macromolecules. *Science* **271,** 67–69 (1996).
3. Cha, J. N. Silicatein filaments and subunits from a marine sponge direct the polymerization of silica and silicones *in vitro*. *Proc. Natl Acad. Sci. USA* **96,** 361–365 (1999).
4. Meldrum, F. C., Mann, S., Heywood, B. R., Frankel, R. B. & Bazylinski, D. A. Electron microscopy study of magnetosomes in two cultured vibrioid magnetotactic bacteria. *Proc. R. Soc. Lond. B* **251,** 238–242 (1993).
5. Colvin, V. L., Goldstein, A. N. & Alivisatos, A. P. Semiconductor nanocrystals covalently bound to metal surfaces with self-assembled monolayers. *J. Am. Chem. Soc.* **144,** 5221–5230 (1992).
6. Brust, M., Bethell, D., Schiffrin, D. J. & Kiely, C. J. Novel gold-dithiol nano-networks with nonmetal electronic properties. *Adv. Mater.* **7,** 795–797 (1995).
7. Li, M., Wong, K. K. W. & Mann, S. Organization of inorganic nanoparticles using biotin-streptavidin connectors. *Chem. Mater.* **11,** 23–26 (1999).
8. Alivisatos, A. P. *et al.* Organization of 'nanocrystal molecules' using DNA. *Nature* **382,** 609–611 (1996).
9. Mirkin, C. A., Letsinger, R. L., Mucic, R. C. & Storhoff, J. J. A DNA-based method for rationally assembling nanoparticles into macroscopic materials. *Nature* **382,** 607–609 (1996).
10. Brown, S. Engineered iron oxide-adhesion mutants of the *Escherichi coli* phage λ receptor. *Proc. Natl Acad. Sci. USA* **89,** 8651–8655 (1992).
11. Brown, S. Metal-recognition by repeating polypeptides. *Nature Biotechnol.* **15,** 269–272 (1997).
12. Parmley, S. F. & Smith, G. P. Antibody-selectable filamentous Fd phage vectors- affinity purification of target genes. *Gene* **73,** 305–318 (1988).
13. Swaminathan, V. & Macrander, A. T. *Materials Aspects of GaAs and InP Based Structures* (Prentice Hall, Englewood Cliffs, New Jersey, 1991).

Acknowledgements

We thank D. Margolese, D. Morse and G. Stucky for discussions, and H. Reese, J. English and R. Naone for providing semiconductor substrates. We acknowledge the use of the core microscopy facilities in the Texas Materials Institute (SEM). We also thank the Institute of Molecular and Cellular Biology (TEM) at the University of Texas at Austin. We acknowledge the assistance of the NSF-sponsored National Nanofabrication Users Network in providing some of the structures for this project. This work was supported by ARO/DARPA (S.R.W and A.M.B), a DuPont Young Investigator Award (A.M.B.), the NSF (P.F.B. and E.L.H.) and the Robert A. Welch Foundation (P.F.B. and A.M.B.). This work was also funded by faculty start-up funds provided by the University of Texas at Austin (A.M.B.).

Correspondence and requests for materials should be addressed to A.M.B. (e-mail: belcher@mail.utexas.edu).

Reduced growth of Alaskan white spruce in the twentieth century from temperature-induced drought stress

Valerie A. Barber*†‡, Glenn Patrick Juday†‡ & Bruce P. Finney*

** Institute of Marine Science, † Forest Sciences Department, University of Alaska Fairbanks, Fairbanks, AK 99775, USA*
‡ These authors contributed equally to the work

The extension of growing season at high northern latitudes seems increasingly clear from satellite observations of vegetation extent and duration[1,2]. This extension is also thought to explain the observed increase in amplitude of seasonal variations in atmospheric CO_2 concentration. Increased plant respiration and photosynthesis both correlate well with increases in temperature this century and are therefore the most probable link between the vegetation and CO_2 observations[3]. From these observations[1,2], it has been suggested that increases in temperature have stimulated carbon uptake in high latitudes[1,2] and for the boreal forest system as a whole[4]. Here we present multi-proxy tree-ring data (ring width, maximum late-wood density and carbon-isotope composition) from 20 productive stands of white spruce in the interior of Alaska. The tree-ring records show a strong and consistent relationship over the past 90 years and indicate that, in contrast with earlier predictions, radial growth has decreased with increasing temperature. Our data show that temperature-induced drought stress has disproportionately affected the most rapidly growing white spruce, suggesting that, under recent climate warming, drought may have been an important factor limiting carbon uptake in a large portion of the North American boreal forest. If this limitation in growth due to drought stress is sustained, the future capacity of northern latitudes to sequester carbon may be less than currently expected.